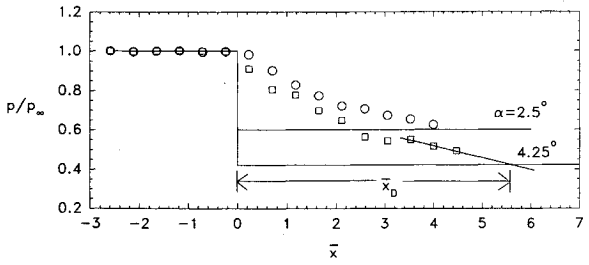

Fig. 3 Surface pressure distribution of turbulent flow past 2.5- and 4.25-deg expansion corners at Mach 8.

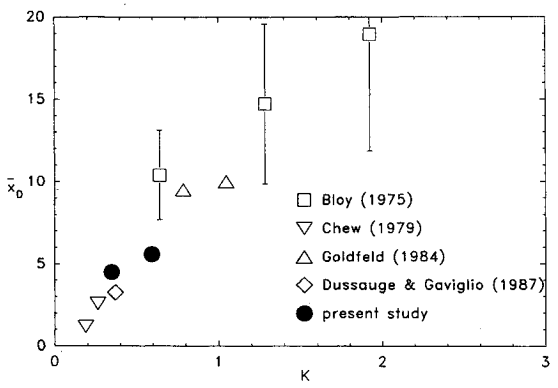

Fig. 4 Downstream influence in turbulent flow past expansion corners.

counterparts. These facts have to be borne in mind when comparing data obtained at low and high Mach numbers.

Downstream Influence Scaling

The mean surface pressure distribution for the two test cases, normalized by a static pressure measured $2.6\delta_0$ upstream of the corner, are plotted in Fig. 3 against $\bar{x} = x/\delta_0$, where x is the streamwise surface coordinate centered at the corner and δ_0 is the undisturbed boundary-layer thickness at the corner location. Also shown in this figure are the inviscid pressure distributions for an incoming Mach 8 flow. No upstream influence of the corner is detected, an observation consistent with previous turbulent studies.[3-5] This is unlike laminar flows where the corner exerts an upstream influence.[9,10] The measured pressures approach the downstream inviscid values some distance $\bar{x}_D = x_D/\delta_0$ from the corners, although adequate downstream data could not be obtained due to model limitations. (The pressure decay should strictly be asymptotic to the downstream inviscid value.) The "downstream influence" of the corner x_D was estimated as that from the corner to the intersection of the tangent through the downstream pressure data with the inviscid downstream pressure as depicted in Fig. 3. The present data show that the larger the corner angle, the stronger the expansion, and thus the longer the downstream influence.

It was thought that the downstream influence depends primarily on an inviscid parameter characterizing the expansion process, namely K.[11] Therefore, the downstream influence data are plotted together with data extracted from previous investigations in Fig. 4. Bloy's data[1] showed excessive scatter and are included simply to reveal the trend of $\bar{x}_D$ with higher values of K. The collapse of data from Mach 1.76–8 supports the validity of K as a scaling parameter, at least for x_D up to $K \approx 1$ where reliable data exist. This validity is particularly striking between the fairly good collapse of Dussauge and Gaviglio's[5] downstream influence with one of the present test cases for approximately the same value of K. It can also be seen from Fig. 4 that the surface pressure of weak expansions reaches the downstream inviscid value quickly. These weak conditions can be achieved at low supersonic Mach numbers even for considerably large corner angles as in the case of Dussauge and Gaviglio.[5] In the past, this has led to the conclusion that the surface pressure reaches the downstream inviscid value in a distance of about one incoming boundary-layer thickness.[2]

Acknowledgments

The research was supported by NASA Langley Grant NAG 1-891 monitored by J. P. Weidner. The authors acknowledge the assistance of E. G. Pace and J. M. Dodson II with some of the experiments.

References

[1]Bloy, A. W., "The Expansion of a Hypersonic Turbulent Boundary Layer at a Sharp Corner," *Journal of Fluid Mechanics,* Vol. 67, Pt. 4, 1975, pp. 647–655.

[2]Narasimha, R., and Viswanath, P. R., "Reverse Transition at an Expansion Corner in Supersonic Flow," *AIAA Journal,* Vol. 13, No. 5, 1975, pp. 693–695.

[3]Chew, Y. T., "Shockwave and Boundary Layer Interaction in the Presence of an Expansion Corner," *Aeronautical Quarterly,* Vol. XXX, Aug. 1979, pp. 506–527.

[4]Goldfeld, M. A., "On the Reverse Transition of Compressible Turbulent Boundary Layer in a Transverse Flow Around a Convex Corner Configuration," *Proceedings of the IUTAM Symposium on Laminar-Turbulent Transition, July 9–13, 1984,* edited by V. V. Kozlov, Springer-Verlag, Berlin, Germany, 1985, pp. 515–520.

[5]Dussauge, J. P., and Gaviglio, J., "The Rapid Expansion of a Supersonic Turbulent Flow: Role of Bulk Dilatation," *Journal of Fluid Mechanics,* Vol. 174, Jan. 1987, pp. 81–112.

[6]Smith, D. R., and Smits, A. J., "The Rapid Expansion of a Turbulent Boundary Layer in a Supersonic Flow," *Theoretical and Computational Fluid Dynamics,* Vol. 2, 1990, pp. 319–328.

[7]Anderson, J. D., Jr., *Hypersonic and High Temperature Gas Dynamics,* McGraw-Hill, New York, 1989, pp. 40–43.

[8]Chung, K.-M., "Shock Impingement Near Mild Hypersonic Expansion Corners," Ph.D. Dissertation, Univ. of Texas at Arlington, Arlington, TX, Dec. 1992.

[9]Bloy, A. W., and Georgeff, M. P., "The Hypersonic Laminar Boundary Layer Near Sharp Compression and Expansion Corners," *Journal of Fluid Mechanics,* Vol. 63, Pt. 3, 1974, pp. 431–447.

[10]Rizzetta, D. P., Burgraff, O. R., and Jenson, R., "Triple-Deck Solutions for Viscous Supersonic and Hypersonic Flow Past Corners," *Journal of Fluid Mechanics,* Vol. 89, Pt. 3, 1978, pp. 535–552.

[11]Stollery, J. L., and Bates, L., "Turbulent Hypersonic Viscous Interaction," *Journal of Fluid Mechanics,* Vol. 63, Pt. 1, 1974, pp. 145–156.

Flow of Rarefied Gas past a Liquid Sphere

Masatugu Tomoeda*
Kumamoto Institute of Technology, Kumamoto 860, Japan

Introduction

THE slow flow past a liquid drop has been studied by many authors because of its fundamental importance in engineering applications. In particular, the rarefied gas flow past a liquid drop will be encountered in various processes such as extraction and atomization of small liquid particles whose characteristic lengths are relatively small compared with the molecular mean free path of the surrounding gas. For very small values of the Weber number, $W_e = \rho_\infty d u_\infty^2/\sigma$, where ρ_∞ and u_∞ are the uniform flow density and velocity, and d

Received Nov. 26, 1991; revision received May 28, 1992; accepted for publication June 5, 1992.

*Associate Professor, Department of Structural Engineering, 4-22-1 Ikeda. Member AIAA.

and σ are the characteristic length and surface tension of the drop, respectively, the drop will be spherical and then deformed into an oblate spheroid with an increase in W_e.

In this Note, we consider a perfectly spherical drop that is placed in the unbounded slow flow of rarefied gas in the near-continuum regime. In comparison with the flow past a solid sphere, the flow under consideration is solved together with the internal circulating motion of the liquid itself induced by the frictional forces acting at the sphere surface.

Mathematical Analysis

Figure 1 shows the geometric configuration of the flows, both inside and outside the sphere, in which the flows are assumed axisymmetric so that flow properties such as the velocities and pressures are determined in terms of the nondimensional radial distance R that is a ratio of the radial distance r to the sphere radius a and the azimuthal angle θ.

Ignoring the inertial effect, the internal flow is governed by the Stokes equations of motion that may be expressed by the following fourth-order differential equation:

$$\delta^4 \Psi_i = 0 \tag{1}$$

where δ is a differential operator defined as

$$\delta^2 = \frac{\partial^2}{\partial R^2} + \frac{1-\alpha^2}{R^2}\frac{\partial^2}{\partial \alpha^2}, \qquad \alpha = \cos\theta \tag{2}$$

and Ψ_i is the nondimensional stream function such that

$$U_{Ri} = -\frac{S}{R^2}\frac{\partial \Psi_i}{\partial \alpha}, \qquad U_{\theta i} = -\frac{S}{\sqrt{1-\alpha^2}}\frac{\partial \Psi_i}{R\,\partial R} \tag{3}$$

In Eq. (3), S is the speed ratio ($S = u_\infty/C_{m\infty}$), $C_{m\infty}$ being the most probable molecular speed of the external gas (or the "thermal speed"), and the subscript i indicates the internal flow.

For the external flowfield around the sphere, macroscopic flow properties such as the flow velocity, the pressure, and the number density will vary significantly for a distance apart in the order of a few mean free paths. The conventional fluid dynamic equations fail to describe the flow and the kinetic theory analysis will be required to solve the Boltzmann equation. Owing to the complexity of the collision term contained in the Boltzmann equation, it is difficult to solve it directly. At present, we employ the Bhatnagar et al.[1] and Welander[2] (BGKW) model that is derived as a relaxation model of the collision term. Since the perturbation of the macroscopic flow properties is small for the flow under consideration, we linearize the BGKW model equation in terms of the nondimensional perturbation of these quantities. Using the spherical coordinate system in the six-dimensional phase space (R, θ, ϕ; Ξ_R, Ξ_θ, Ξ_ϕ), the linearized BGKW model equation may be written in the following form[3]:

$$K\Delta\Phi + \Phi = 2(\Xi_R U_R + \Xi_\theta U_\theta) + N + (\Xi^2 - 3/2)\Theta$$

$$\Xi^2 = \Xi_R^2 + \Xi_\theta^2 + \Xi_\phi^2 \tag{4}$$

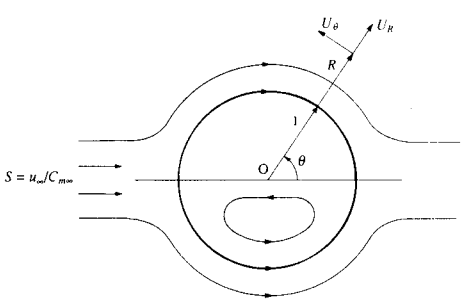

Fig. 1 Geometry of the flows.

where $U(U_R, U_\theta, 0)$ and $\Xi(\Xi_R, \Xi_\theta, \Xi_\phi)$ are the flow velocity and the molecular velocity, respectively, nondimensionalized with respect to $C_{m\infty}$, and the subscripts R, θ, and ϕ, respectively, denote the components in the direction of radial distance, azimuthal angle, and longitudinal angle. The flow velocity component U_ϕ is set equal to zero for axisymmetry as mentioned previously. The symbol Δ is a differential operator defined as

$$\Delta = \Xi_R\frac{\partial}{\partial R} - \Xi_\theta\frac{\sqrt{1-\alpha^2}}{R}\frac{\partial}{\partial \alpha} + (\Xi_\theta^2 + \Xi_\phi^2)\frac{\partial}{R\,\partial \Xi_R} + \left(\Xi_\phi^2\frac{\alpha}{\sqrt{1-\alpha^2}} - \Xi_R\Xi_\theta\right)\frac{\partial}{R\,\partial \Xi_\theta} - \Xi_\phi\left(\Xi_R + \Xi_\theta\frac{\alpha}{\sqrt{1-\alpha^2}}\right)\frac{\partial}{R\,\partial \Xi_\phi} \tag{5}$$

and K is the Knudsen number defined here as

$$K = \frac{\lambda_\infty}{a} \tag{6}$$

where λ_∞ is the molecular mean free path.

The quantity Φ in Eq. (4) is the nondimensional perturbation distribution function such that

$$(1+\Phi)F_0 = \frac{C_{m\infty}^3}{n_\infty}f, \qquad F_0 = \pi^{-3/2}\exp(-\Xi^2) \tag{7}$$

where f is the molecular distribution function and n the number density. The other nondimensional quantities that appeared in Eq. (4) are defined as follows:

$$N = \frac{n - n_\infty}{n_\infty} \tag{8a}$$

$$\Theta = \frac{T - T_\infty}{T_\infty} \tag{8b}$$

$$P = \frac{p - p_\infty}{p_\infty} = N + \Theta \tag{8c}$$

where T and p are the temperature and the pressure, respectively.

The macroscopic properties N, U, and P(or Θ) are to be determined by the following integrals:

$$N = \iiint \Phi F_0\, d\Xi \tag{9a}$$

$$U = \iiint \Xi\Phi F_0\, d\Xi \tag{9b}$$

$$P = \frac{2}{3}\iiint \Xi^2\Phi F_0\, d\Xi \tag{9c}$$

where

$$d\Xi = d\Xi_R\, d\Xi_\theta\, d\Xi_\phi \tag{10}$$

and the integrals are carried over all molecular velocity ranges ($-\infty < \Xi_R, \Xi_\theta, \Xi_\phi < \infty$).

Multiplying both sides of Eq. (4) by 1, Ξ, and $\frac{1}{2}\Xi^2$ and integrating over all of the molecular velocity ranges yields Maxwell's transport equations, i.e., the conservation equations of mass, momentum, and energy, respectively, in the nondimensional form.

The boundary conditions are given as follows:

1) At the center of the sphere ($R = 0$), the flow velocity remains finite, i.e.,

$$-\infty < U_{Ri},\ U_{\theta i} < \infty \tag{11}$$

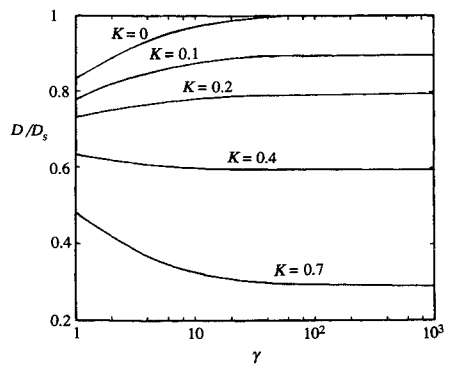

Fig. 2 Variation of sphere drag with viscosity ratio.

2) At the surface of the sphere ($R = 1$): a) The molecules are assumed to reflect completely diffusely with the temperature equal to that of the uniform flow of the gas, which may be described by the Maxwellian distribution function in the nondimensional form:

$$\Phi = \Phi_w = N_w + 2\Xi_\theta U_{\theta i} \qquad \text{for} \qquad \Xi_R > 0 \tag{12}$$

where the subscript w denotes the surface condition. b) It is assumed that there is no net mass flux, i.e.,

$$U_R = \int\int\int \Xi_R \Phi_{R=1} F_0 \, d\Xi = 0 \tag{13}$$

c) The continuity of the shear stress holds between the liquid and the gas:

$$\int\int\int \Xi_R \Xi_\theta \Phi_{R=1} F_0 \, d\Xi = -\frac{\mu_i u_\infty}{2p_\infty a}\left[\frac{\sqrt{1-\alpha^2}}{R^2}\frac{\partial^2 \Psi_i}{\partial \alpha^2} - \frac{1}{\sqrt{1-\alpha^2}} R \frac{\partial}{\partial R}\left(\frac{\partial \Psi_i}{R^2 \partial R}\right)\right]_{R=1} \tag{14}$$

3) At infinity ($R \to \infty$), the external flow asymptotically approaches the undisturbed uniform flow condition that may be expressed as

$$(U_R, U_\theta) = S(\alpha, -\sqrt{1-\alpha^2}) \tag{15}$$

To solve the external flow, we divide it into two flow regions, i.e., the asymptotic region, where the variation of the flow is gradual with respect to the mean free path and the flow is essentially governed by the hydrodynamic equations, and the Knudsen layer region in the immediate vicinity of the sphere surface, where the flow properties vary significantly with respect to the mean free path. The solution for each region is obtained using the matched asymptotic expansion method.

In the asymptotic region, $K\Delta\Phi$ in Eq. (4) is of higher order than the remaining terms. Thus, the nondimensional distribution function Φ may be expanded[3] in terms of K, which will be retained here to the order of K. Substituting Φ thus obtained into Maxwell's transport equations for momentum previously mentioned gives rise to the Stokes equations of motion that may be written in terms of the nondimensional stream function Ψ as

$$\delta^4 \Psi = 0 \tag{16}$$

Solving Eqs. (1) and (16) together with the boundary conditions, Eqs. (11) and (15), yields the stream functions Ψ and Ψ_i written as

$$\Psi = \frac{1}{2}\left[R^2 - \left(\frac{3}{2} - \frac{A + 2B + 2C_i}{2}\right)R + \left(\frac{1}{2} + \frac{A + 2B + 2C_i}{2}\right)\frac{1}{R}\right](1-\alpha^2) \tag{17a}$$

$$\Psi_i = \tfrac{1}{2} C_i (R^4 - R^2)(1-\alpha^2) \tag{17b}$$

where A, B, and C_i are the integral constants. The constants A and B are of $\mathcal{O}(K)$ and may be expanded into series in terms of K as

$$A = KA_1 + K^2 A_2 + \cdots \tag{18a}$$

$$B = KB_1 + K^2 B_2 + \cdots \tag{18b}$$

where $A_1, B_1, \ldots,$ are numerical values related to the discontinuity of the flow velocity components U_R and U_θ, respectively, at the surface and will be determined by means of the kinetic theory analysis. On the other hand, the constant C_i indicates the liquid flow at the surface and can be evaluated from the continuity of shear stress, Eq. (14), which is reduced to

$$\int\int\int \Xi_R \Xi_\theta \Phi_{R=1} F_0 \, d\Xi = \frac{3}{2} \gamma \, SKC_i \sqrt{1-\alpha^2} \tag{19}$$

where γ is the viscosity ratio given by

$$\gamma = \frac{\mu_i}{\mu} \tag{20}$$

The properties, U_R, U_θ, P, Θ, and N in the asymptotic field are then determined as

$$U_R = S\left[1 - \left(\frac{3}{2} - \frac{A + 2B + 2C_i}{2}\right)\frac{1}{R} + \left(\frac{1}{2} + \frac{A - 2B - 2C_i}{2}\right)\frac{1}{R^3}\right]\alpha \tag{21a}$$

$$U_\theta = -S\left[1 - \left(\frac{3}{4} - \frac{A + 2B + 2C_i}{4}\right)\frac{1}{R} - \left(\frac{1}{4} + \frac{A - 2B - 2C_i}{4}\right)\frac{1}{R^3}\right]\sqrt{1-\alpha^2} \tag{21b}$$

$$P = -SK\left(\frac{3}{2} - \frac{A + 2B + 2C_i}{2}\right)\frac{\alpha}{R^2} \tag{21c}$$

$$\Theta = SKC_0 \frac{\alpha}{R^2} \tag{21d}$$

$$N = -SK\left(\frac{3}{2} - \frac{A + 2B - 2C_0 + 2C_i}{2}\right)\frac{\alpha}{R^2} \tag{21e}$$

To analyze the Knudsen layer region, we define a Knudsen variable D such that

$$R = 1 + KD, \qquad 0 \le D \le \mathcal{O}(1) \tag{22}$$

Then Eq. (4) may be rewritten as

$$\Xi_R \frac{\partial \Phi}{\partial D} + \Phi + \frac{K}{1+KD}\left[-\sqrt{1-\alpha^2}\Xi_\theta \frac{\partial \Phi}{\partial \alpha} + (\Xi_\theta^2 + \Xi_\phi^2)\frac{\partial \Phi}{\partial \Xi_R} + \left(\frac{\alpha}{\sqrt{1-\alpha^2}}\Xi_\phi^2 - \Xi_R \Xi_\theta\right)\frac{\partial \Phi}{\partial \Xi_\theta} - \Xi_\phi\left(\Xi_R + \frac{\alpha}{\sqrt{1-\alpha^2}}\right)\frac{\partial \Phi}{\partial \Xi_\phi}\right] = 2(\Xi_R U_R + \Xi_\theta U_\theta) + N + \left(\Xi^2 - \frac{3}{2}\right)\Theta \tag{23}$$

Replacing R in the asymptotic solutions, Eqs. (21a-21e), by Eq. (22) and expanding them for small values of KD results in those written in terms of the Knudsen variable D. We also expand the nondimensional distribution function Φ in Eq. (23), where we retain terms of order up to K.

The constants A (or A_1, A_2, . . .) and C_i appearing in Eqs. (21) can now be determined from the surface conditions,

Eqs. (13) and (19), respectively. To the order of terms to be retained here, they are found to be

$$A_1 = 0 \tag{24a}$$

$$C_i = \frac{1}{2(1+\gamma)} \tag{24b}$$

Using the asymptotic solutions thus obtained and the surface condition, Eq. (12), as the boundary conditions for $D \to \infty$ and at $D = 0$, respectively, the differential equation, Eq. (23), is now integrated to obtain the nondimensional distribution function Φ. It is then introduced into the integrals, Eqs. (9), to determine the flow properties N, U, and P (or Θ), where we expand them into a series of functions, $J_n(D)$, ($n = 1, 2, 3, \ldots$), defined as

$$J_n(D) = \int_0^\infty x^n \exp\left(-x^2 - \frac{x}{D}\right) dx \tag{25}$$

All of the coefficients contained in the flow properties may be determined numerically by applying the moment method,[3] i.e., multiplying both sides of Eqs. (9) by $D^l (l = 0, 1, 2, \ldots)$ and integrating them with respect to D from $D = 0$ to ∞ gives rise to simultaneous linear equations for those constants.

Drag of a Liquid Sphere

As a final solution, the drag of a liquid sphere is determined by integrating the momentum flux[3] over the entire sphere surface and found to be

$$D = D_s\left(1 - \frac{2}{3} C_i - \frac{2}{3} KB_1\right) \tag{26}$$

where D_s is the conventional Stokes drag given by

$$D_s = 6\pi\mu u_\infty a \tag{27}$$

Figure 2 shows dependence of the drag ratio D/D_s on γ with K as a parameter. In this figure, increasing values of γ indicate that effects of the internal circulation decrease and that the flow behavior essentially approaches that for a solid sphere. In the case of $K = 0$, which implies the continuum flow, the drag ratio is somewhat smaller than unity for small values of γ, suggesting the effect of the internal circulation. The drag ratio then approaches unity as the value of γ increases. For other values of K, the rarefaction of the external flow effectively diminishes the drag ratio, which is interpreted as the effect of the velocity slip at the sphere surface. This rarefaction effect is more pronounced for larger values of γ as indicated in the case of $K = 0.7$.

Conclusions

The kinetic theory analysis was carried out to investigate the slow flow of rarefied gas past a liquid spherical drop. The linearized BGKW model of the Boltzmann equation was employed to solve the flow outside the sphere, and the analysis was extended to the first order of the Knudsen number. The circulating internal flow of liquid within the sphere was also analyzed. As a result, it was found that the significant internal circulation would occur when the viscosity of the external gas and that of the internal liquid are comparable to each other in magnitude. This results in reduction of the sphere drag from the conventional Stokes drag. The rarefaction of the external flow also has a decreasing effect on the drag by the order of the Knudsen number, which is greater for larger values of the viscosity ratio between the internal liquid and the external gas.

References

[1]Bhatnagar, P. L., Gross, E. P., and Krook, M., "A Model for Collision Processes in Charged and Neutral One-Component Systems," *Physical Review*, Vol. 94, No. 3, 1954, pp. 511-525.

[2]Welander, P., "On the Temperature Jump in a Rarefied Gas," *Arkiv for Physik*, Vol. 7, No. 44, 1954, pp. 507-553.

[3]Tomoeda, M., "A Theoretical and Experimental Study on the Flow of Rarefied Gas Past a Sphere," Univ. of Toronto Inst. for Aerospace Studies, UTIAS Rept. 216, Toronto, Ontario, Canada, May 1977.

Comparison of Chemical Kinetic Rate Mechanisms for High-Temperature Air, Including Electronic Energy

Yvette Weber* and John Anderson Jr.†
University of Maryland,
College Park, Maryland 20742

Introduction

THE purpose of this work is to examine and compare the behavior of several chemical kinetic models in high-temperature air that are currently popular for modern high-temperature flowfield analyses and also to examine the effect of simultaneously assuming a finite equilibrium electronic energy. For this investigation a sample gas dynamic model is used, namely, the inviscid, nonequilibrium chemically reacting flowfield downstream of a normal shock wave in air. This flow is calculated using both the Dunn and Kang and the Park kinetic mechanisms. Local thermodynamic equilibrium is assumed in all calculations. Comparisons are made between results obtained from both models along with results obtained from a hybrid model that applies Gupta's curve fits for the equilibrium constants of the reactions. Calculations are performed with and without the inclusion of equilibrium electronic energy as part of the mixture enthalpy. Results show that, although the different kinetic models tend toward the same equilibrium condition far downstream, the rates of chemical relaxation can vary widely between models. Also, the addition of the electronic energy is shown to produce only small changes in the flowfield properties and species mass fractions.

Contents

Over the past several years there has been much interest in the design of high Mach number, high-altitude vehicles such as the aeroassisted space transfer vehicle (ASTV). Under these conditions, it is likely that the flowfield will be in local chemical and thermal nonequilibrium and that a significant portion of the heat transfer will come from radiative nonequilibrium.[1] Since these nonequilibrium processes affect the performance of the vehicle, it is important that they be investigated and that the extent to which they dominate the flowfield be known. Thus, many recent studies have focused on the computation of such flowfields around complex geometries. Although these studies are necessary and valuable, the complexity of the physical processes and numerical solution introduce much uncertainty. The processes of molecular transport, chemical kinetics, and radiative heating must be sufficiently understood and modeled. In addition, numerical issues such as grid convergence and temporal accuracy must also be considered. Moreover, because of the amount of computer time required, these studies are generally performed at only a few design points in the vehicle trajectory.

Received Oct. 14, 1991; accepted for publication Feb. 21, 1992.

*DOD Graduate Fellow, Department of Aerospace Engineering. Student Member AIAA.

†Professor, Department of Aerospace Engineering. Fellow AIAA.